Landau theory of cholesteric blue phases: The role of higher harmonics

H. Grebel
Department of Electronics, The Weizmann Institute of Science, Rehovot 76100, Israel

R. M. Hornreich*
Department of Mathematics, Imperial College of Science and Technology, University of London, London SW7 2BZ, England and Department of Theoretical Physics, University of Oxford, Oxford OX1 3NP, England

S. Shtrikman†
Department of Electrical Engineering and Computer Science, University of California, San Diego, La Jolla, California 92093

(Received 16 April 1984)

The Landau theory of blue phases (BP) in cholesteric liquid systems is further developed by systematically including the effect of higher harmonics in the structure factor on the free energy. The inclusion of a third harmonic results in two new body-centered-cubic (bcc) structures, O_b^8 and O_c^8, in addition to the bcc O^5 ($I432$) and O_a^8 ($I4_132$) and simple-cubic O^2 ($P4_232$) structures previously obtained [Phys. Rev. A **28**, 1114 (1983)] in the two-harmonic framework. Introducing a fourth harmonic does not lead to any further structures or significant changes in the free energies. Detailed results of the Landau-theory calculations are compared with experimental data and those obtained with other models. It is shown that, in general, the observed properties of BP I and BP II are consistent with the structure assignment BP I$\leftrightarrow O_c^8$ and BP II$\leftrightarrow O^2$. Some points requiring further investigation and clarification are indicated.

I. INTRODUCTION

It is now generally accepted that the blue phases (BP)[1,2] which appear in many cholesteric liquid crystals below their clearing point possess cubic orientational order (not, however, the "gray" of "fog" phase, also known as BP III). Using Landau theory, we have shown[2] that such ordered structures are indeed thermodynamically stable in certain regions of the temperature-chirality plane. Our approach was as follows. Taking as our order parameter the anisotropic part of the dielectric tensor

$$\epsilon_{ij}(\vec{r}) \equiv \epsilon_{ij}^{d}(\vec{r}) - \tfrac{1}{3}\mathrm{Tr}(\epsilon^{d})\delta_{ij} , \tag{1}$$

we formally expanded $\epsilon_{ij}(\vec{r})$ in a Fourier series. Initially, we restricted ourselves to considering only those contributions to the Fourier sum associated with a set of wave vectors having equal magnitudes. This procedure, which is *asymptotically exact* in the high-chirality (short-pitch) regime, yielded a transition from the isotropic (I) phase to one having a body-centered-cubic structure belonging to the space group O^5 ($I432$). This structure, however, is *not* the thermodynamically stable one at physically interesting values of the cholesteric pitch, due to the significant role played by Fourier components of $\epsilon_{ij}(\vec{r})$ associated with harmonics of the basic spatial wave vector. By explicit calculation we showed that even the addition of a *single* harmonic results in the appearance of new structures. Significantly, we found[2] that structures belonging to both body-centered-cubic O^8 ($I4_132$) and simple-cubic O^2 ($P4_232$) space groups become stable in regions of the phase diagram of experimental interest.

These results naturally lead one to wonder what the effect of *additional* harmonics would be on the theoretical phase diagram. However, direct analytic calculations of the Landau free energy become extremely time-consuming as additional Fourier components of $\epsilon_{ij}(\vec{r})$ are taken into account. We have therefore developed a different approach, combining symmetry considerations and numerical techniques, to greatly reduce the complexity of the calculation. Using this procedure, the contributions of additional harmonics can be systematically incorporated into the Landau free energy. We here present results obtained by including up to *four* different wave-vector magnitudes (i.e., fundamental and three harmonics) in the Fourier sum.

This paper is organized as follows. In Sec. II we calculate expressions for the free energies of the O^2, O^5, O^8, and usual helicoidal (C) phases as functions of the Fourier amplitudes. We also give here and in Appendix A details of the technique employed. Then, in Sec. III, we discuss the minimization of the free energies and obtain the thermodynamic phase diagram in the temperature-chirality plane. Models of the various BP structures are also presented. Section IV is devoted to a detailed comparison of our results with the experimental data and other theoretical calculations. A critical summary with emphasis on outstanding questions is given in the concluding section.

II. CALCULATION OF THE FREE ENERGIES

For cholesteric systems, the average free-energy density is given by[2,3]

$$F = V^{-1}\int d\vec{r}\,[\tfrac{1}{2}(a\epsilon_{ij}^2 + c_1\epsilon_{ij,l}^2 + c_2\epsilon_{ij,i}\epsilon_{lj,l} - 2de_{ijl}\epsilon_{in}\epsilon_{jn,l}) - \beta\epsilon_{ij}\epsilon_{jl}\epsilon_{li} + \gamma(\epsilon_{ij}^2)^2]\,, \tag{2}$$

where, as usual, a is proportional to a reduced temperature, c_1, c_2, d, β, and γ are temperature-independent parameters, $\epsilon_{ij,l}\equiv\partial\epsilon_{ij}/\partial x_l$, and we sum on repeated indices. For thermodynamic stability it is necessary that c_1, γ, and $c_1+\frac{2}{3}c_2$ be positive.[2,3] Expanding

$$\epsilon_{ij}(\vec{r}) = \sum_{h,k,l} N^{-1/2}\epsilon_{ij}(\sigma)\exp[iq(hx+ky+lz)]\,, \tag{3}$$

with $\sigma = h^2+k^2+l^2$, $N = 3!2^{3-n_0}/n_1!$, where n_0 (n_1) is the number of vanishing (equal) $|h|, |k|, |l|$, and, for *each* $[hkl]$ (including [000])

$$[\epsilon(\sigma)] = \sum_{m=-2}^{2}\epsilon_m(\sigma)e^{i\psi_m(hkl)}[M_m(hkl)] = \frac{1}{2}\left[\epsilon_2 e^{i\psi_2}\begin{pmatrix}1 & i & 0\\ i & -1 & 0\\ 0 & 0 & 0\end{pmatrix} + \epsilon_1 e^{i\psi_1}\begin{pmatrix}0 & 0 & 1\\ 0 & 0 & i\\ 1 & i & 0\end{pmatrix} + \sqrt{\tfrac{2}{3}}\epsilon_0 e^{i\psi_0}\begin{pmatrix}-1 & 0 & 0\\ 0 & -1 & 0\\ 0 & 0 & 2\end{pmatrix} + \epsilon_{-1}e^{i\psi_{-1}}\begin{pmatrix}0 & 0 & -1\\ 0 & 0 & i\\ -1 & i & 0\end{pmatrix} + \epsilon_{-2}e^{i\psi_{-2}}\begin{pmatrix}1 & -i & 0\\ -i & -1 & 0\\ 0 & 0 & 0\end{pmatrix}\right], \tag{4}$$

with $\epsilon_m(\sigma)\geq 0$ and $\psi_m(hkl) = -\psi_m(\bar{h}\bar{k}\bar{l})$. The basis matrices $[M_n]$ are defined such that $[hkl]$ is the polar axis of a local coordinate system which is defined separately for each $[hkl]$. These $[M_m]$ matrices are in fact isomorphous to the five $j=2$ spherical harmonics.

Using (2)–(4), the harmonic part of F is easily found to be[2]

$$F_2 = \tfrac{1}{2}\sum_{\sigma,m}\{a - mdq\sigma^{1/2} + [c_1 + \tfrac{1}{6}c_2(4-m^2)]q^2\sigma\}\epsilon_m^2(\sigma)\,. \tag{5}$$

Since, in Landau theory, we ignore any explicit q dependence of higher than second-order contributions, we have $\partial F/\partial q = \partial F_2/\partial q$ and, from (5),

$$r = q/q_0 = \left[\sum_{\sigma,m}[m\sigma^{1/2}\epsilon_m^2(\sigma)]\right] \Big/ \left[\sqrt{2}\sum_{\sigma,m}\{[1+\tfrac{1}{6}(4-m^2)c_2/c_1]\sigma\epsilon_m^2(\sigma)\}\right], \tag{6}$$

with $q_0\equiv d/\sqrt{2}c_1$. The $\sigma=0$ term is excluded from the sums in (6).

The excitation spectrum for a chiral ($d\neq 0$) system is shown in Fig. 1. Note that the stability condition $c_1+\frac{2}{3}c_2>0$ guarantees that the ground state lies on the $m=2$ branch (for $d>0$) of the excitation spectrum.

We shall here consider order parameters whose energetically significant Fourier amplitudes belong exclusively to the low-lying ($m=2$ for $d>0$) branch of the excitation spectrum. In this case the c_2 term in (2) does not contribute [see (5)] and we can simplify our notation by introducing the scaled quantities[2]

$$\epsilon_{ij} = s\mu_{ij},\quad s = \beta/\sqrt{6}\gamma,\quad f = F/(\beta^4/36\gamma^3)\,,$$
$$\tfrac{1}{4}t = (3\gamma/\beta^2)a,\quad \tfrac{1}{4}\xi_R^2 = (3\gamma/\beta^2)c_1\,, \tag{7}$$
$$\kappa = q_C\xi_R = \sqrt{2}q_0\xi_R\,.$$

Note that $q_C = d/c_1$ is the wave vector of the usual cholesteric (helicoidal) phase, which is characterized by a single nonzero wave vector. Substituting (7) into (2) and using (5) gives

$$f = \tfrac{1}{4}\sum_{\sigma}\left[t - \kappa^2 + \kappa^2(\sigma^{1/2}r/\sqrt{2}-1)^2\mu_2^2(\sigma) + V^{-1}\int d\vec{r}\,[-\sqrt{6}\mu_{ij}\mu_{jl}\mu_{li} + (\mu_{ij}^2)^2]\right]. \tag{8}$$

We shall now use (3) and (4) (with ϵ replaced by μ) to calculate f for a restricted number of terms in the Fourier sum. Before doing this, however, we determine the phases $\psi_2(hkl)$. For a given space group these phases are *not* independent of each other and symmetry considerations can be used to simplify the free-energy calculations considerably. We therefore proceed by analyzing separately the three cubic space groups of interest: O^2, O^5, and O^8. In each case we restrict ourselves to the contributions of the

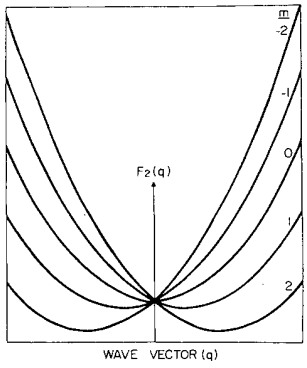

FIG. 1. Wave vector (q) and eigenvalue (m) dependence of the quadratic part of the Landau free energy for a cholesteric liquid crystal.

four lowest-lying independent Fourier amplitudes to the free energy.

(1) O^2: For *all* simple cubic groups the four lowest-lying states correspond to $\sigma=1$, 2, 3, and 4. For O^2, however, occupation of the $m=2,\sigma=3$ and 4 harmonics is *forbidden* by symmetry[2,4] and $\mu_2(3)=\mu_2(4)=0$. Thus only two amplitudes need be considered explicitly. This case has been treated previously[2] and it is therefore sufficient to summarize the results. Phases are fixed by setting the origin of the coordinate frame at the point (000) in the O^2 unit cell[5] with point-group symmetry 23 (T). The threefold [111] symmetry axis passes through this point and it immediately follows that there are at most *three* independent phases, $\psi_2(100)$, $\psi_2(110)$, and $\psi_2(\bar{1}10)$. All others are determined by cyclic permutation. Next, as a consequence of the fourfold screw-axis symmetry, $\psi_2(110)=\psi_2(\bar{1}10)$. Finally, the twofold symmetry with respect to the coordinate axes requires that each phase be equal to its negative and all phases are therefore either 0 or π. The choice in each case is determined by our convention that the Fourier amplitudes $\mu_2(1)$ and $\mu_2(2)$ be positive at the free-energy minimum. In fact, since even powers of $\mu_2(1)$ appear in f, only $\psi_2(110)$ need be fixed.[6] By setting it equal to π, the expression for the normalized free energy is[2]

$$f_{O^2}=\tfrac{1}{4}[t-\kappa^2+\kappa^2(r/\sqrt{2}-1)^2]\mu_2^2(1)+\tfrac{1}{4}[t-\kappa^2+\kappa^2(r-1)^2]\mu_2^2(2)-[3(4+3\sqrt{2})/8]\mu_2^2(1)\mu_2(2)$$
$$+(23\sqrt{2}/32)\mu_2^3(2)+\tfrac{13}{12}\mu_2^4(1)+[(139-12\sqrt{2})/48]\mu_2^2(1)\mu_2^2(2)+\tfrac{499}{384}\mu_2^4(2)\ , \tag{9a}$$

with, from (6),

$$r=\sqrt{2}[\mu_2^2(1)+\sqrt{2}\mu_2^2(2)]/[\mu_2^2(1)+2\mu_2^2(2)]\ . \tag{9b}$$

(2) O^5: For *all* body-centered-cubic groups the four lowest-lying states are those with $\sigma=2$, 4, 6, and 8. In the case of O^5, the $m=2,\sigma=2$ state is forbidden,[2,4] thus $\mu_2(4)=0$. Setting our origin at the point (000) in the O^5 unit cell[5] with point-group symmetry 432 (O), it is straightforward to show that (a) all other phases are related to $\psi_2(110)$, $\psi_2(\bar{1}10)$, $\psi_2(112)$, $\psi_2(1\bar{1}2)$, $\psi_2(\bar{1}12)$, $\psi_2(\bar{1}\bar{1}2)$, $\psi_2(220)$, and $\psi_2(\bar{2}20)$ by permutation symmetry, (b) $\psi_2(110)=\psi_2(\bar{1}10)$, $\psi_2(112)=\psi_2(1\bar{1}2)=\psi_2(\bar{1}12),=\psi_2(\bar{1}\bar{1}2)$, and $\psi_2(220)=\psi_2(\bar{2}20)$ due to the fourfold symmetry, and (c) the remaining independent phases $\psi_2(110)$, $\psi_2(112)$, and $\psi_2(220)$ must be equal to either 0 or π as a consequence of the twofold symmetry.

Setting all phases equal to zero, the expression for the free energy was obtained by constructing analytically the explicit real-space matrices $\mu_{ij}(\vec{r};\sigma)$ for *each* value of σ (here 2, 6, and 8) separately and using (8). We divided the integrals in (8) into subsets of the form

$$I_3(\sigma_1,\sigma_2,\sigma_3)=\eta_3 V^{-1}\int d\vec{r}\,\mu_{ij}(\vec{r};\sigma_1)\mu_{jl}(\vec{r};\sigma_2)\mu_{li}(\vec{r};\sigma_3)\ , \tag{10}$$

$$I_4(\sigma_1,\sigma_2,\sigma_3,\sigma_4)=\eta_4 V^{-1}\int d\vec{r}\,\mu_{ij}(\vec{r};\sigma_1)\mu_{ij}(\vec{r};\sigma_2)\times\mu_{ln}(\vec{r};\sigma_3)\mu_{ln}(\vec{r};\sigma_4)\ .$$

Here $\eta_3=3!/n_1!$ and $\eta_4=4!/n_1!n_2!$, where n_1 and n_2 are the number of equal σ_i. Finally, the integrals I_3 and I_4 were evaluated numerically by sampling the unit cell at $(25)^3$ equally spaced points. As checks on the numerical accuracy of this technique (a) the relevant computer results for I_3 and I_4 were compared with those found in analytic studies[2] of O^2, O^5, and O^8 with one and two wave-vector magnitudes and (b) the remaining I_3 integrals were also computed analytically. In all cases there was agreement to seven significant figures.

The resulting expression for the O^5 phase-normalized free-energy density is

$$F_{O^5}=\tfrac{1}{4}\sum_\sigma[t-\kappa^2+\kappa^2(\sigma^{1/2}r/\sqrt{2}-1)^2]\mu_2^2(\sigma)-1.016\,466\mu_2^3(2)-0.421\,875\mu_2^3(6)-1.016\,466\mu_2^3(8)$$
$$-1.305\,769\mu_2^2(2)\mu_2(6)+0.879\,653\mu_2^2(6)\mu_2(8)+1.611\,463\mu_2(2)\mu_2^2(6)$$
$$+3.265\,544\mu_2(2)\mu_2(6)\mu_2(8)+1.299\,479\mu_2^4(2)+1.435\,925\mu_2^4(6)+1.299\,479\mu_2^4(8)$$
$$+0.791\,441\mu_2^3(2)\mu_2(6)-0.656\,250\mu_2^3(2)\mu_2(8)+0.434\,449\mu_2^3(6)\mu_2(8)-0.428\,002\mu_2(2)\mu_2^3(6)$$
$$+2.915\,720\mu_2^2(2)\mu_2^2(6)+2.890\,625\mu_2^2(2)\mu_2^2(8)+2.341\,443\mu_2^2(6)\mu_2^2(8)$$
$$-0.362\,657\mu_2^2(2)\mu_2(6)\mu_2(8)-0.137\,340\mu_2(2)\mu_2^2(6)\mu_2(8)-0.854\,748\mu_2(2)\mu_2(6)\mu_2^2(8)\ , \tag{11a}$$

with

$$r=\sqrt{2}\left[\sum_\sigma\sigma^{1/2}\mu_2^2(\sigma)\right]\Big/\left[\sum_\sigma\sigma\mu_2^2(\sigma)\right]\ . \tag{11b}$$

The sums in (11) are restricted to $\sigma=2$, 6, and 8.

(3) O^8: This group, like O^5, is body-centered cubic and thus the four lowest-lying states are again $\sigma=2$, 4, 6, and 8. However, *all* these values are now symmetry allowed.[2,4] The determination of the phases $\psi_2(hkl)$ is more complex for this structure and is given in Appendix A. We show there that

$$\begin{aligned}
&\psi_2(110)=-\psi_2(\bar{1}10)-\pi/2=0 \text{ or } \pi \ , \\
&\psi_2(200)=-\pi/2 \text{ or } +\pi/2 \ , \\
&\psi_2(112)=\psi_2(\bar{1}\bar{1}2)=-\psi_2(1\bar{1}2)-\pi/2=\psi_2(\bar{1}12)-\pi/2=0 \text{ or } \pi \ , \\
&\psi_2(220)=\psi_2(\bar{2}20)+\pi=0 \text{ or } \pi \ .
\end{aligned} \tag{12}$$

All other phases are related to the above by cyclic permutation of the (hkl) indices.

Choosing in each case the first-mentioned allowed value for the phase angle, the third- and fourth-order terms in (8) were computed using the same technique discussed previously. The resulting expression for the free energy is

$$\begin{aligned}
f_{O^8}=&\tfrac{1}{4}\sum_{\sigma}[t-\kappa^2+\kappa^2(\sigma^{1/2}r/\sqrt{2}-1)^2]\mu_2^2(\sigma)-0.625\,000\mu_2^3(2)-0.421\,875\mu_2^3(6)+1.016\,466\mu_2^3(8) \\
&-2.185\,660\mu_2^2(2)\mu_2(4)-1.305\,769\mu_2^2(2)\mu_2(6)-3.090\,990\mu_2^2(4)\mu_2(8) \\
&+0.879\,653\mu_2^2(6)\mu_2(8)+0.101\,175\mu_2(2)\mu_2^2(6)+2.146\,521\mu_2(4)\mu_2^2(6)+3.039\,058\mu_2(2)\mu_2(4)\mu_2(6) \\
&-2.638\,958\mu_2(2)\mu_2(6)\mu_2(8)+1.169\,271\mu_2^4(2)+1.083\,333\mu_2^4(4)+1.312\,918\mu_2^4(6) \\
&+1.299\,479\mu_2^4(8)+1.000\,867\mu_2^3(2)\mu_2(4)-0.342\,005\mu_2^3(2)\mu_2(6)+0.530\,330\mu_2^3(2)\mu_2(8) \\
&+0.976\,298\mu_2^3(6)\mu_2(8)+0.554\,214\mu_2(2)\mu_2^3(6)-0.981\,769\mu_2(4)\mu_2^3(6)+3.499\,387\mu_2^2(2)\mu_2^2(4) \\
&+2.291\,159\mu_2^2(2)\mu_2^2(6)+2.713\,542\mu_2^2(2)\mu_2^2(8)+3.280\,513\mu_2^2(4)\mu_2^2(6)+2.542\,280\mu_2^2(4)\mu_2^2(8) \\
&+4.273\,114\mu_2^2(6)\mu_2^2(8)-0.143\,613\mu_2^2(2)\mu_2(4)\mu_2(6)+1.717\,217\mu_2^2(2)\mu_2(4)\mu_2(8) \\
&-1.038\,890\mu_2^2(2)\mu_2(6)\mu_2(8)+1.733\,969\mu_2(2)\mu_2^2(4)\mu_2(6)-2.164\,614\mu_2(2)\mu_2(4)\mu_2^2(6) \\
&+1.380\,818\mu_2(2)\mu_2^2(6)\mu_2(8)-1.729\,131\mu_2(2)\mu_2(6)\mu_2^2(8)-2.968\,469\mu_2(4)\mu_2^2(6)\mu_2(8) \\
&-2.473\,295\mu_2(2)\mu_2(4)\mu_2(6)\mu_2(8) \ ,
\end{aligned} \tag{13a}$$

with

$$r=\sqrt{2}\left[\sum_{\sigma}\sigma^{1/2}\mu_2^2(\sigma)\right]\Big/\left[\sum_{\sigma}\sigma\mu_2^2(\sigma)\right] . \tag{13b}$$

The sums in (13) are restricted to $\sigma=2$, 4, 6, and 8.

(4) C: For completeness we also give the result for the usual cholesteric (helicoidal) phase. The expression for the normalized free-energy density is[2]

$$\begin{aligned}
f_c=&\tfrac{1}{4}t\mu_0^2(0)+\tfrac{1}{4}(t-\kappa^2)\mu_2^2(2)+\mu_0^3(0) \\
&-3\mu_0(0)\mu_2^2(2)+[\mu_0^2(0)+\mu_2^2(2)]^2 \ .
\end{aligned} \tag{14}$$

III. THERMODYNAMIC PHASE DIAGRAM

In the preceding section we presented expressions for the free energies of four possible ordered phases in cholesteric liquid crystals. One of these (O^2) has a nonsymmorphic simple-cubic (sc) structure, another (O^5) is symmorphic body-centered cubic (bcc), the third (O^8) is nonsymmorphic and body-centered cubic, and the fourth (C) is the usual helicoidal cholesteric structure. In addition, of course, there is the isotropic (I) or disordered phase with $F_I=0$ which is always the thermodynamically stable state at sufficiently high temperatures. Our objective is to determine which of these five phases is the thermodynamically stable one at any arbitrary point (t,κ) in the temperature-chirality plane. This is done by minimizing, for given (t,κ), the free energy functions (9), (11), (13), and (14) and then choosing the structure whose $f_{\min}$ is lowest. The minimization was carried out numerically using gradient search routines. Both analytic and numerical computations of the gradient vector were employed and were found to give identical results. Since gradient searches yield only local minima, it was necessary, particularly in the case of O^8, to carry out a systematic search for the global minimum by initiating the search procedure at different points in the parameter space.

The results can be summarized as follows.

(1) O^2: The minimization of (9) with respect to the parameters $\mu_2(1)$ and $\mu_2(2)$ presented no difficulties as only

one minimum with $\mu_2(1),\mu_2(2)\neq 0$ was found at all (t,κ) regardless of the initial starting point. In all cases, $\mu_2(1)$ and $\mu_2(2)$ were positive at $(f_{O^2})_{\min}$, thus $\psi_2(\sigma=2)=\pi$ is the proper setting. Some typical results are listed in Table I. Note that $r/\sqrt{2}$ rather than r is given as, in the case of sc symmetry, this is the relative shift of the longest wavelength Bragg reflection with respect to that of the C phase.

(2) O^5: The free energy (11) was minimized with respect to the three parameters $\mu_2(2)$, $\mu_2(6)$, and $\mu_2(8)$. As in the case of O^2, only one minimum with nonzero Fourier amplitudes was found for all (t,κ). At the minima, $\mu_2(2)$ and $\mu_2(6)$ were always positive, thus the corresponding phases are indeed zero. For $\mu_2(8)$, on the other hand, the appropriate choice of the associated phase $\psi_2(220)$ is (t,κ) dependent. The higher-order amplitudes always satisfied $\mu_2(6)<0.15\mu_2(2)$ and $\mu_2(8)<0.04\mu_2(2)$; thus the effect of including harmonics on the structure and free energy of the O^5 phase is small. In particular, the fourth ($\sigma=8$) harmonic is negligible. Some results are given in Table I. Note that where the amplitude $\mu_2(8)$ is enclosed in parenthesis, $\psi_2(220)=\pi$. Otherwise, all phases are equal to zero.

(3) O^8: The minimization of (13) with respect to the four parameters $\mu_2(2)$, $\mu_2(4)$, $\mu_2(6)$, and $\mu_2(8)$ was much more complicated than the corresponding calculations for the other phases. As an intermediate step, we therefore set $\mu_2(8)=0$ and carried out a three parameter search. *Three* local minima were found (as compared with one when only two amplitudes were considered[2]) in various regions of the (t,κ) plane and a systematic choice of initial starting points was used in order to locate the global minimum with certainty. The fourth amplitude was then also allowed to vary. This resulted in very small changes in the positions in parameter space and associated free energies of the three local minima, but *no* additional minima were found. This indicates that incorporating three Fourier amplitudes in the order parameter suffices to locate *all* the free-energy minima of the O^8 structure, with the fourth amplitude serving only to refine the energy calculation.

It is useful to discuss the three relative minima of (13) separately. We begin by noting that, when only *two* Fourier amplitudes were taken into account,[2] a single minima was found with positive amplitudes for $\psi_2(110)=0$, $\psi_2(\bar{1}10)=\psi(200)=-\pi/2$. In this structure, which we shall henceforth refer to as O_a^8, the amplitude ratio $\mu_2(4;O_a^8)/\mu_2(2;O_a^8)$ was approximately $\frac{1}{2}$. Including the $\sigma=6$ and 8 harmonics, we find that O_a^8 is the energetically preferred O^8 structure *only* in a restricted region of the phase diagram just below the clearing point (see Fig. 2). An example given in Table I is at $t=1.7$, $\kappa=0.9$. As before, O_a^8 is characterized by $\mu_2(4;O_a^8)/\mu_2(2;O_a^8)\simeq\frac{1}{2}$ with much smaller contributions (less than 7%) from the $\sigma=6$ and 8 harmonics. In all cases, the amplitudes are

TABLE I. Fourier amplitudes $\mu_m(\sigma)$, frequency shift r (for O^2, $r/\sqrt{2}$), and reduced free energy f of the cubic phases O^2, O^5, O_a^8, O_b^8, O_c^8, and helicoidal phase C at selected points (t,κ) in the theoretical phase diagram. The appropriate choice of phase angles is summarized in Table V. Note the alternate choice for those amplitudes given in parentheses.

	$\kappa=0.9$				$\kappa=1.3$				$\kappa=1.5$			
t:	1.1	1.2	1.6	1.7	0.6	2.5	2.6		0.1	0.4	2.9	3.1
O^2												
$\mu_2(1)$	0.53	0.52	0.42	0.39	0.71	0.41	0.37		0.80	0.78	0.45	0.39
$\mu_2(2)$	0.30	0.29	0.24	0.22	0.39	0.23	0.21		0.43	0.42	0.25	0.22
$r/\sqrt{2}$	0.89	0.89	0.89	0.89	0.89	0.89	0.89		0.89	0.89	0.89	0.89
$10f$	−0.44	−0.35	−0.056	−0.002	−2.19	−0.032	+0.018		−4.13	−3.52	−0.12	−0.003
	O_b^8	O_b^8	O_b^8	O_a^8	O_b^8	O^5	O^5	O_a^8	O_b^8	O_b^8	O^5	O^5
$\mu_2(2)$	0.54	0.53	0.43	0.33	0.72	0.43	0.39	0.32	0.82	0.79	0.48	0.42
$\mu_2(4)$	0.02	0.02	0.03	0.16	0.01	0	0	0.15	0.01	0.01	0	0
$\mu_2(6)$	0.25	0.24	0.18	0.01	0.33	0.06	0.06	0.00	0.38	0.36	0.06	0.06
$\mu_2(8)$	0.10	0.10	0.08	0.02	0.12	(0.02)	(0.02)	0.02	0.12	0.12	0.01	0.01
r	0.81	0.81	0.82	0.90	0.82	0.97	0.97	0.91	0.83	0.83	0.98	0.98
$10f$	−0.42	−0.33	−0.042	−0.003	−2.11	−0.041	+0.003	+0.011	−4.00	−3.40	−0.12	−0.02
O_c^8												
$\mu_2(2)$	0.45	0.44	0.36	0.32	0.60	0.33	0.29		0.69	0.67	0.37	0.30
$\mu_2(4)$	0.35	0.33	0.28	0.26	0.45	0.27	0.24		0.51	0.50	0.30	0.26
$\mu_2(6)$	0.23	0.22	0.18	0.16	0.30	0.16	0.14		0.33	0.32	0.18	0.15
$\mu_2(8)$	0.00	0.01	0.01	0.01	(0.00)	0.02	0.02		0.00	0.00	0.02	0.02
r	0.77	0.77	0.77	0.77	0.78	0.77	0.77		0.78	0.78	0.77	0.77
$10f$	−0.44	−0.35	−0.048	+0.006	−2.19	−0.014	+0.033		−4.14	−3.52	−0.09	+0.02
C												
$\mu_0(0)$	0.31	0.29	0.24	0.21	0.39				0.44	0.42		
$\mu_2(2)$	0.58	0.52	0.45	0.40	0.76				0.86	0.83		
$10f$	−0.45	−0.35	−0.013	+0.045	−2.19				−4.13	−3.46		

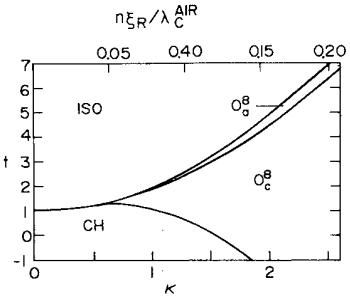

FIG. 2. Theoretical phase diagram when only the I, C, and three O^8 phases (O_a^8,O_b^8,O_c^8) are allowed. Here λ_C^{AIR} is the C-phase Bragg back-reflection wavelength in air, n is the index of refraction, and ξ_R is a racemic mixture correlation length at the phase transition. All boundaries denote first-order phase transitions.

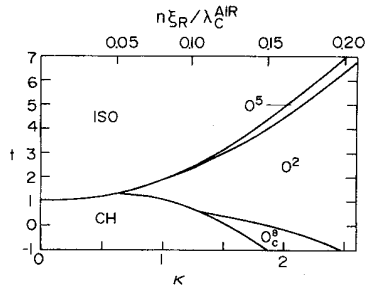

FIG. 3. Theoretical phase diagram when all *seven* phases, I, C, O^2, O^5, O_a^8, O_b^8, and O_c^8 are allowed. The notation is as in Fig. 2.

positive for the choice of phase angles used in (13).

In addition to O_a^8, we find *two* other *locally* stable O^8 structures. The first, which we shall refer to as O_b^8, is similar to O_a^8 in that its Fourier amplitudes are also all positive for the phase angles used in (13). It differs from O_a^8 primarily in that the second Fourier amplitude $\mu_2(4;O_b^8)$ essentially vanishes. That is $\mu_2(4;O_b^8)/\mu_2(2;O_b^8)<0.07$ while $\mu_2(6;O_b^8)/\mu_2(2;O_b^8)\simeq 0.5$ (see Table I). Note that the fourth harmonic is not negligible, as $\mu_2(8;O_b^8)/\mu_2(2;O_b^8)$ can be as large as 0.2. Finally, the third O^8 structure, which we call O_c^8, is quite different from either O_a^8 or O_b^8. In this case, the fundamental amplitude $\mu_2(2,O_c^8)$ is *negative* for the choice of phase angles in (13) and it is therefore necessary to set $\psi_2(110)=-\psi_2(\bar{1}10)-\pi/2=\pi$ for O_c^8. [This is equivalent to replacing $\mu_2(2)$ by its negative in (13).] The phase of the fourth harmonic is (t,κ) dependent for O_c^8; where $\mu_2(8)$ is enclosed in parentheses in Table I, the correct choice is $\psi_2(220)=\psi_2(\bar{2}20)+\pi=\pi$. In any case, this harmonic is negligible.

When *only* the phases I, C, and O^8 are considered, the phase diagram shown in Fig. 2 is obtained. In general, for fixed κ, the transitions are from $I\rightarrow O_a^8\rightarrow O_c^8\rightarrow C$ as the temperature decreases. The O_b^8 structure does not appear.

When all *seven* structures (I, O^2, O^5, O_a^8, O_b^8, O_c^8, and C) are considered, we obtain the phase diagram shown in Fig. 3. It contains five phases [the O_a^8 structure is, in addition, thermodynamically stable in an extremely narrow region ($\Delta t<0.02$) for $\kappa\simeq 0.9$ just below the clearing point (e.g., at $t=1.7$, $\kappa=0.9$ as given in Table I)], including the O^2, O^5, and O_c^8 cubic structures. Of these three, sc O^2 has the dominant position. As expected,[2] body-centered-cubic O^5 appears immediately below the isotropic phase and above O^2 for sufficiently large κ (here, $\kappa\gtrsim 1$). More important is the appearance of a bcc (O_c^8) structure between O^2 and C for $\kappa\gtrsim 1.3$.

We stress, however, that the energy differences between the various cubic structures is relatively small. This is particularly true of O^5-O^2 and O^2-O_c^8, respectively. To illustrate this point we show, in Figs. 4(a)–(c), those regions in which the free-energy differences between these phases are less than 0.5%, 1%, and 2%, respectively. (The clearing-point free energy is set to zero for this purpose.) Note particularly the sensitivity of the O^2-O_c^8 phase boundary to small shifts in the free energies. Also, although the O_b^8 structure does not appear in the thermodynamic phase diagram, its free energy, particularly near the O^2-C phase boundary (see Table I) is only 4% to 5% greater than that of O^2. We shall return to these points in Sec. IV.

Until now we have concentrated on the symmetries of the different structures. One may also ask what they actually look like, i.e., how does the local molecular orientation change with position within a unit cell? A useful qualitative picture can be obtained by utilizing a concept introduced earlier[7] in which the order parameter is constrained to be locally uniaxial and cubic lattices are obtained by packing space with arrays of interlaced right-circular cylinders, in each of which the uniaxial director describes a "curling-mode" configuration. A locally uniaxial order parameter has the form

$$\epsilon_{ij}(\vec{r})=(\tfrac{3}{2})^{1/2}\epsilon(\vec{r})[n_i(\vec{r})n_j(\vec{r})-\tfrac{1}{3}\delta_{ij}]\ , \tag{15}$$

with $\hat{n}^2=1$. In the curling mode[7] (also referred to as "double twist"[8]) the director configuration can be written in cylindrical coordinates (r,θ,z) as

$$\hat{n}=\hat{\theta}\sin\omega+\hat{z}\cos\omega\ , \tag{16}$$

with ω and ϵ independent of θ and z. Using (15) and (16) with appropriate boundary conditions, an isolated single cylinder with this configuration has been shown to be a rigorous minimum of the Landau free-energy functional (2) under certain conditions.[9] This solution is shown schematically in Fig. 5.

A sc O^2 structure can be formed using these cylinders by interlacing them in the manner shown in Fig. 6(a). Note that the directors in adjacent units should coincide at the contact points and have continuous first derivatives.[7] In fact, the two-harmonic Landau-theory solution for the O^2 structure order parameter, obtained by minimizing (9) and using (2), is similar to Fig. 6(a). The main differences occur in the small intercylinder regions, where the Landau solution is strongly biaxial. In a strictly uniaxial approach, these biaxial regions must be regarded as disordered and $\langle 111\rangle$ direction disclinations are then introduced into the model.[8,10]

A skeleton bcc structure, compatible with O_c^8, can be obtained from the O^2 one in Fig. 6(a) by removing, simul-

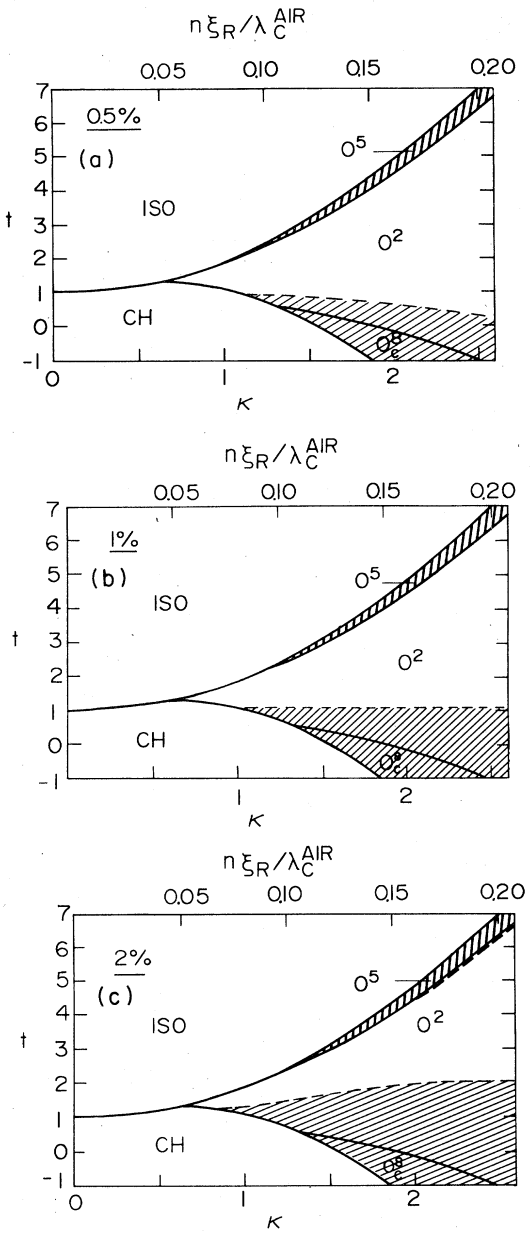

FIG. 4. Theoretical phase diagram showing those regions in which the free energies of adjoining cubic phases differ by less than (a) 0.5%, (b) 1%, (c) 2%. The free-energy zero is at the clearing point. The notation is as in Fig. 2.

taneously, alternate curling-mode cylinders along the three crystallographic axes. O_a^8 and O_b^8, on the other hand, are qualitatively modeled by the very different array shown in Fig. 6(b). (This figure is somewhat closer to the O_b^8 Landau-theory solution for the order parameter than that for O_a^8.) The O_a^8,O_b^8 array and one corresponding to O_c^8 will differ strongly as, in one case (O_c^8), cylinders will lie along ⟨100⟩ axes, while in the other (O_a^8,O_b^8) they will be along ⟨111⟩. Alternately, the disclinations (which necessarily occur in strictly uniaxial models) would lie along ⟨111⟩ and ⟨100⟩, respectively.[10] Nevertheless,

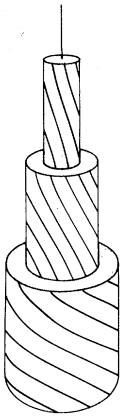

FIG. 5. Schematic illustration of the cylindrically symmetric spatially localized minimum Landau free-energy structure found in Ref. 9. The director describes a curling-mode configuration.

both are invariant under the operations of the O^8 space group.

The O^5 structure differs from O^2 and O^8 in that it is symmorphic and cannot be modeled by an array of interlaced but nonintersecting cylinders. It necessarily contains, even in biaxial models, points at which the system remains disordered. In fact, these defect points define the vertices of a bcc lattice and the earliest suggestion[11] of an O^5 BP structure was formulated on this basis. A model of the Landau-theory solution for O^5 has been given elsewhere.[12(c)] The biaxial regions are located essentially on the ⟨111⟩ axes, which become disclinations in a uniaxial model.[8,10]

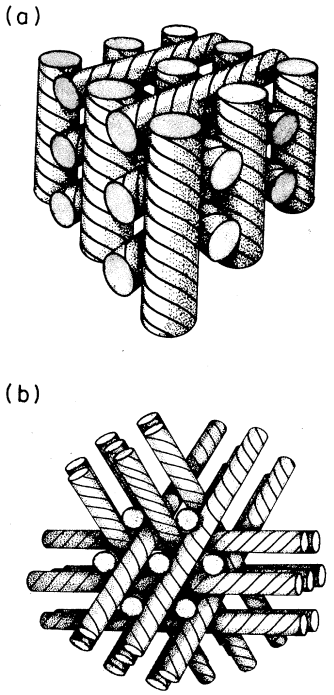

FIG. 6. The (a) O^2 and (b) O_a^8,O_b^8 cubic structures, showing how they can be visualized as appropriate interlaced assemblies of the curling-mode configuration cylinders of Fig. 5.

IV. COMPARISON WITH EXPERIMENT

In the previous sections we have expanded the Landau theory of phase transitions in cholesterics so as to systematically include the effects of higher harmonics on the structure factors of the cubic phases and their free energies. Before undertaking a detailed comparison with experiment we note that the Landau theory of cholesterics has *already* provided[2] an explanation for many of the observed properties of BP, including the following.

(1) The narrowing and eventual disappearance of the BP with increasing pitch (i.e., decreasing κ).[1,13–15]

(2) The relative narrowness of the BP region. Experimentally, the correlation length ξ_R defined in (7) is approximately[16] 25 nm and the index of refraction[14] $n \simeq 1.6$. The C-phase Bragg back-reflection wavelength[1,13–15] in air $\lambda_c^{\rm AIR} = 4\pi n/q_C = 370$ to 600 nm and, from (7), $\kappa = 4\pi n \xi_R / \lambda_C^{\rm AIR} \simeq 0.8$ to 1.4. The reduced temperature scale unit is the extrapolated-from-the-disordered phase-transition temperature for a racemic mixture and, experimentally,[17] is 0.5–1 K. From Fig. 3 it then follows that the theoretical width of the measured BP region is 1–2 K, in excellent agreement with experiment.[1,13–15]

(3) All cubic phases (including O^2, O^5, and O^8) will exhibit many of the experimentally observed optical properties of BP I and BP II, including absence of birefringence,[1] optical activity,[1] and Bragg scattering.[1,13–15]

(4) The existence of more than one cubic BP. As discussed in the Introduction and Sec. II, the inclusion of *one* additional harmonic in the order parameter was shown[2] to result in O^2 and O_a^8, in addition to O^5, becoming thermodynamically stable. However, these results were not sufficient to allow a complete correlation of all the properties of the observed phases with the model predictions. While the known BP properties were, in many respects, compatible with an assignment of O^8 for BP I and O^2 for BP II, there were several inconsistencies, particularly between O_a^8 and BP I.

We now compare the more detailed results obtained in this paper with the experimental data. As an aid to the experimentalist, we also reformulate the Landau free energy (2) in terms of experimentally accessible quantities in Appendix B.

A. Phase diagram

Experimentally at least two distinct phases exhibiting Bragg scattering are known to exist between the isotropic and helicoidal ones. With increasing temperature, $C \rightarrow$BP I$\rightarrow$BP II$\rightarrow I$. [An additional amorphouslike phase, BP III, which is found between BP II and I, will be discussed shortly.] In the case of BP II the first two Bragg peaks have been observed, while for BP I as many as four have been found.[1,13,14,18,19] The observation of a strong second Bragg reflection for both BP indicates that neither of these phases has an O^5 structure, since $\epsilon_2(\sigma=2;O^5)=0$. Even more definitely, the polarized light studies of Flack and Crooker[14] eliminate any identification of BP I or BP II with O^5, as they found that the second Bragg line is strongly sensitive to the sense of circularly polarized input light. Rigorous selection rules,[2,4] completely *independent* of model calculations, require that any O^5 $\sigma=2$ reflection be polarization independent in back reflection.

A comparison of Fig. 3 with the experimental phase sequence $C \rightarrow$BP I$\rightarrow$BP II$\rightarrow I$ clearly requires us to identify with BP I with O_c^8 and BP II with O^2. Although Fig. 3 indicates that O_c^8 appears only for $\kappa \gtrsim 1.3$, the extremely small energy difference between O_c^8 and O^2 (see Fig. 4) means that small contributions [from, e.g., adding higher-order terms to the basic Landau free-energy functional (2)] could shift the O^2-O_c^8 phase boundary significantly. Such terms lead, for example, to anisotropy in the Frank elastic constants.[20] They could also result in the appearance of O_c^8 at lower values of κ.

As regards the phase diagram then, the remaining open point is the apparent nonappearance of an O^5 phase between BP II (O^2) and the disordered phase for $\kappa \gtrsim 1$. As noted, very small changes in the free energies would result in O^5 appearing only at much higher values of κ. Also, this is the region in which Marcus and Goodby[15] found amorphous BP III. It thus appears that for intermediate chiralities this amorphous phase could have a lower free energy than O^5. It has been suggested[9] that BP III could be a *disordered* collection of the curling-mode cylinders illustrated in Fig. 5, which then form into ordered arrays at slightly lower temperatures. Clearly, a spatially nonperiodic minimum of the Landau free-energy functional deserves further study as a potential BP structure.

B. Bragg intensities

As already noted, O^5 can be eliminated as the structure of either BP I or BP II since both these phases exhibit polarization-sensitive second Bragg peaks.[14] Moreover, the observation that the first four peaks of BP I are all polarization sensitive[14] eliminates *any* sc (including, of course, O^2) structure for this phase.[2,4] This conclusion is based upon general optical selection rules[4] and *not* upon particular model calculations. These calculations, however, allow us, in addition, to compare theoretical polycrystalline Bragg intensities with those found experimentally by Meiboom and Sammon,[13] as given in Table I of Ref. 10. Their data were taken by measuring the nonscattered or transmitted intensity as a function of incident beam wavelength λ. In this configuration, there is a series of steps (reductions) in the transmitted intensity with decreasing λ, each step occurring when the Bragg condition for backscattering at a given σ is satisfied. For a polycrystalline sample and nonpolarized incident flux I_0, the change in the total scattered intensity at *each* Bragg backscattering in the weak scattering (thin sample) limit is[4(b)]

$$\Delta\Phi_T(\sigma) = (\pi^2 N^2 V / 8 n^4 \lambda_\sigma) \epsilon_2^2(\sigma) I_0 , \tag{17}$$

where N is the multiplicity [see (3)], V the scattering volume, n the index of refraction, and $\lambda_\sigma = 4\pi/q\sigma^{1/2}$. In (17), only the dominant $m=2$ contribution to the scattering is given.

From (17), the intensity ratio of steps at σ_1 and σ_2 (for *fixed* I_0) is

TABLE II. Comparison of observed and calculated relative Bragg intensities.

Reflection number	Observed[a] BP I	BP II	Calculated[b] O^2	O^5	O_a^8	O_b^8	O_c^8	Calculated[c] O^2	O^5	O_b^8 (O^{8+})	O_c^8 (O^{8-})
1	1	1	1	1	1	1	1	1	1	1	1
2	0.54	0.29	0.42	0	0.30	(0)	0.79	0.30	0	0.01	0.53
3	0.20	<0.05	0	0.05	(0)	0.35	0.42	0	(0)	0.13	0.22
4	<0.05	<0.05	0	(0)	(0)	0.06	(0)	0	0.05	(0)	(0)

[a]From Ref. 10, Table I.
[b]Landau-theory calculation; from Eq. (18) of this paper. The values given are, to within ±5%, independent of t and κ. The rotation (0) indicates values below 0.01.
[c]Disclination-theory calculation; from Ref. 10, Table I.

$$\Delta\Phi_T(\sigma_2)/\Delta\Phi_T(\sigma_1)=\lambda_{\sigma_2}^{-1}\epsilon_2^2(\sigma_2)/\lambda_{\sigma_1}^{-1}\epsilon_2^2(\sigma_1)$$
$$=\sigma_2^{1/2}\epsilon_2^2(\sigma_2)/\sigma_1^{1/2}\epsilon_2^2(\sigma_1)\ . \qquad (18)$$

In principle, however, (18) *cannot* be compared directly to the results of Meiboom *et al.*[10,13] for several reasons. These include, first, the strong Bragg scattering observed. This indicates that the thin sample limit is inappropriate and that the sample thickness should be taken into account explicitly.[4(c)] That is, if the sample is regarded as segmented into a smaller number of layers, a nonnegligible portion of the incident beam is scattered in each layer and this significantly affects the amplitude and state of polarization of the beam incident upon succeeding layers. Second, as the incident wavelength is decreased and the second and succeeding backscattering thresholds are reached, the beam is simultaneously Bragg reflected by all the longer wavelengths as well as the new one. This changes the characteristics of the effective incident beam. Third, while only one circularly polarized component of the incident beam is Bragg scattered, both components are affected by wavelength-dependent anomalous scattering and depolarization effects as a consequence of the nonideal nature of the medium. This results in a wavelength-dependent change in incident-beam properties. Finally, multiple scattering of a single Bragg reflection could affect the observed intensities.

An approximate way of taking the first two of the above factors into account is described in Appendix C. The other effects, however, which can also be substantial [see Ref. 4(c) and footnote 18 of Ref. 10], are much more difficult to estimate. We therefore give, in Table II, the calculated relative intensities for the case of a *thin scatterer,* as obtained using (18). We also give, for comparison, the experimental intensity ratios quoted by Meiboom *et al.*[10] together with their calculated intensities. The latter are based upon disclination models for the BP, together with computer solutions of Maxwell's equations to obtain scattering intensities. This approach, of course, is quite different from the one presented here and, in principle, takes sample thickness into account.

From Table II we see that the very different theoretical models results in very similar predictions for the relative scattering intensities of the cubic phases. This similarity is even greater (see Appendix C) when thickness corrections are taken into account. Further, our theoretical results for O^2 and O_c^8 correlate with those for BP II and BP I, respectively. To a lesser degree, O_a^8 intensities are compatible with those of BP II. No correlation is obtained with any of the other theoretical structures. This then supports the phase diagram results of Sec. IV A.

C. Bragg reflection wavelengths: The red shift

Another experimentally accessible quantity is the shift of the primary BP Bragg peak with respect to that of the C phase. The physical origin of this shift was discussed previously[12(c)] and, since it results in an expansion of the lattice, was termed the "red shift." Within the Landau-theory framework, it is closely connected to the Bragg intensities. When only $m=2$ amplitudes need be considered, (6) may be rewritten in the simpler form

$$r=\sqrt{2}\sum_\sigma \sigma^{1/2}\epsilon_2^2(\sigma)\Big/\sum_\sigma \sigma\epsilon_2^2(\sigma)$$
$$=\sqrt{2}\sum_\sigma \Phi(\sigma)\Big/\sum_\sigma \sigma^{1/2}\Phi(\sigma)\ , \qquad (19)$$

TABLE III. Comparison of observed and calculated shifts of the fundamental Bragg back-reflection wavelength of the cubic phases relative to that of the helicoidal phase.

Observed BP I	BP II	Calculated[a] O^2	O^5	O_a^8	O_b^8	O_c^8	Calculated[b] O^2	O^5	O_b^8 (O^{8+})	O_c^8 (O^{8-})
1.27[c]	1.10[c]	1.12	1.03	1.10	1.22	1.29	1.18	1.20	1.20	1.35
1.40[d]	1.24[d]									

[a]Landau-theory calculation; this paper. The values given are essentially independent of t and κ.
[b]Disclination-theory calculation; from Ref. 10, Table II. The values quoted are for the case of equal Frank constants.
[c]From Ref. 13 on cholesterol derivatives.
[d]From Ref. 14 on biphenyls.

where $\Phi(\sigma)$ is the intensity of the σ Bragg peak for a polycrystalline specimen. Noting that the relative wavelength shift is r^{-1} for bcc structures and $(r/\sqrt{2})^{-1}$ for sc ones, we obtain the values given in Table III. Also given are experimental values obtained on cholestrol derivatives[13] and biphenyl compounds,[14] and the equivalent theoretical results of Meiboom *et al.*[8,10] Note that the latter are obtained by a procedure quite different from that given here and do *not* have a direct connection with the Bragg intensities. Comparison of the values for O^5 makes this clear.

From the table we see that our O^2 and O_c^8 theoretical values are in good agreement with those on the cholesterol derivatives and somewhat poorer agreement with those on the biphenyls. Here also the data are consistent with an assignment of the O^2 structure to BP II and the O_c^8 one to BP I.

D. Latent heats

Using high-resolution differential scanning calorimetry, Stegemeyer and Bergmann[1] have measured the relative latent heats of cholesteric nonanoate and myristate associated with the $I\rightarrow$BP II, BP II$\rightarrow$BP I, and BP I$\rightarrow C$ phase transitions. Since all these transitions occur in an extremely narrow temperature range, the latent heat ratios are essentially equal to those of the changes in entropy. These are related to the Landau free energies by

$$\Delta S_{ab}=16\left|\frac{df_b}{dt}-\frac{df_a}{dt}\right|_{t=t_{ab}}, \tag{20}$$

where the prefactor has been fixed so that $\Delta S_{IC}(\kappa=0)=1$.

The entropy changes associated with the different phase transitions occurring in the phase diagram (Fig. 3) are shown graphically in Fig. 7. In particular, we note that $\Delta S_{IO^2}/\Delta S_{O^2O_c^8}\simeq 21$ and $S_{O_c^8C}/\Delta S_{O^2O_c^8}\simeq 5$. While the latter ratio is compatible with experiment,[1] the former is low by at least a factor of 5. As pointed out previously,[2] one possible reason for this discrepancy is the use of Landau (i.e., mean-field) theory, in which fluctuation contributions to the entropy changes are neglected. These are likely to be much greater at an $I\rightarrow$BP than at a BP$\rightarrow C$ transition, since the former is order-disorder in character while the latter is between two ordered phases. Thus quantitative comparisons of theoretical latent heat ratios involving an order-disorder transition obtained using Landau theory with experiment are difficult. Quantitatively the results in Fig. 8 are in agreement with the assignment BP II$\leftrightarrow O^2$, BP I$\leftrightarrow O_c^8$. The alternate assignment BP I$\leftrightarrow O_b^8$ would, however, be equally valid.

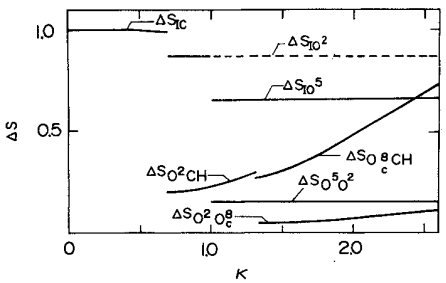

FIG. 7. Entropy changes ΔS associated with the different phase transitions as a function of the chirality parameter κ.

E. Fourier amplitude ratios: Darwin widths

An alternate method of determining relative Fourier amplitudes, based upon Darwin width measurements, has been given by Marcus.[21] Based upon his data, we found[2] for the primary BP reflections

$$\mu(\text{BP II})/\mu(C)=0.41\pm 0.05\ ,$$
$$\mu(\text{BP I})/\mu(C)=0.24\pm 0.05\ . \tag{21}$$

However, this ratio is strongly sensitive to the relative temperatures at which the BP and C-phase reflections are measured. Assuming that the C-phase peak is measured at the BP-C phase boundary, the theoretical Darwin width ratios of the five cubic structures discussed in Secs. II and III lie in the respective ranges:

$$0.31\leq\mu_2(1;O^2)/\sqrt{3}\mu_2(2,C)\leq 0.54\ ,$$
$$0.21\leq\mu_2(2;O^5)/\sqrt{6}\mu_2(2,C)\leq 0.25\ ,$$
$$0.23\leq\mu_2(2;O_a^8)/\sqrt{6}\mu_2(2,C)\leq 0.24\ , \tag{22}$$
$$0.24\leq\mu_2(2;O_b^8)/\sqrt{6}\mu_2(2,C)\leq 0.26\ ,$$
$$0.27\leq\mu_2(2;O_c^8)/\sqrt{6}\mu_2(2,C)\leq 0.32\ .$$

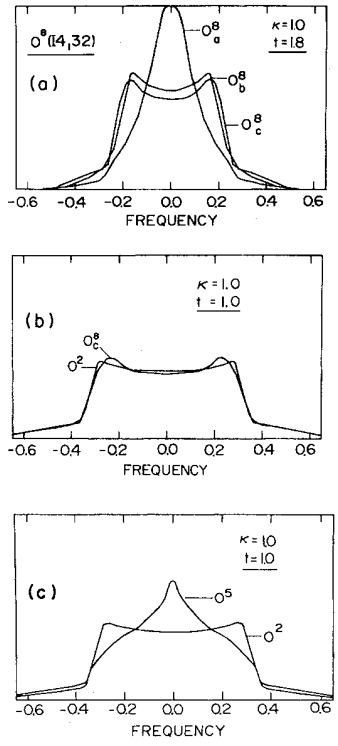

FIG. 8. Theoretical NMR spectra of the (a) O_a^8, O_b^8, O_c^8, (b) O^2, O_c^8, (c) O^2,O^5 phases showing the effect of quadrupolar splitting.

Note that these ranges are for κ values of physical interest and take into account (except for O_b^8) the 2% energy differences shown in Fig. 4(c). For O_b^8, the entire width of the O^8 phase regions shown in Fig. 2 was used.

Comparing (21) with (22), we see that the experimental results are indicative for a sc structure for BP II and a bcc one for BP I. More detailed measurements will be needed in order to differentiate among the different bcc structures by this technique.

F. NMR quadrupolar splittings

The theory of NMR quadrupolar splitting of deuterated cholesteric liquid crystals has been given by us elsewhere.[21] We showed that the I-phase NMR resonance line is *split* when $\mu_{ij} \neq 0$ by a frequency difference proportional to

$$\omega(\vec{x}_0, \{\alpha\}) = \sum_{i,j} \alpha_{\tau i} \mu_{ij} \alpha_{j\tau} , \tag{23}$$

where $\vec{x}_0$ is the site of the deuterated nucleus and $\alpha_{\xi i}$ is the direction cosine between the applied magnetic field direction $\hat{\xi}$ and the $\hat{i}$ axis of the μ_{ij} coordinate frame. Using (23), the theoretical spectrum can be found by calculating the percentage of deuterium nuclei whose quadrupolar splittings lie between ω and $(\omega + \Delta\omega)$. The following procedure was used:

(a) A single unit cell of the O^2, O^5, O_a^8, O_b^8, and O_c^8 structures was sampled using a grid.

(b) The deuterium nuclei were assumed to be uniformly distributed. Molecular diffusion, which may be important,[22] was *not* taken into account.

(c) Polycrystalline samples were simulated by averaging over all orientations $\{\alpha\}$ of μ_{ij} with respect to $\hat{\xi}$ using an appropriate grid.

(d) For each cubic structure, $\mu_{ij}(\vec{r})$ was determined from the appropriate free-energy minimization and Eqs. (3) and (4) (with ϵ replaced by μ).

(e) The ω scale was subdivided and the number of grid points having splittings in each subdivision was calculated. Each spectrum was symmetrized about $\omega = 0$ and, for comparison purposes, the area of each was normalized to unity.

(f) The above procedure was repeated using finer and finer grids until amplitude changes in the calculated spectra were less than 4%.

Some typical theoretical spectra, obtained using the above procedure, are shown in Fig. 8. First, in Fig. 8(a), we compare those of the three O^8 structures. Both the O_b^8 and O_c^8 spectra consist of well-split doublets and are quite distinct from that of O_a^8. The O^2 spectrum [Fig. 8(b)] is also a doublet, with features quite similar to those of O_a^8 and O_c^8. Finally [Fig. 8(c)], we see that the O^5 spectrum is distinctly different from that of O^2 and the other phases shown in Fig. 8(b). Although Fig. 8 gives the spectra of the five cubic phases at only one point in the phase diagram, the essential features of each are in fact *independent* of the particular point chosen.

Experimental BP NMR spectra have been reported by Samulskii and Luz[22] and by Yaniv *et al.*[23] All these spectra have strong similarities to those of Fig. 8(b). No attempt was made to distinguish between BP-I and BP-II spectra and our theoretical results indicate that this may be difficult.

G. Morphology

While the Landau-theory calculations presented here cannot be directly applied to morphology studies, it is nevertheless useful to briefly compare the conclusions reached. Onusseit and Stegemeyer[24] and Marcus[25] have shown that under controlled conditions BP II grows in the form of square platelets. This is associated with a fourfold $\langle 100 \rangle$ symmetry axis normal to the plane of the platelets.[25] When BP II$\rightarrow$BP I, crosshatching is observed within the platelets due to the formation of two equivalent sets of $\{110\}$ planes normal to the observation direction. These results are all consistent with sc and bcc structures for BP II and BP I, respectively, and thus in general agreement with the Landau-theory results. Another interesting point is the observation[1,14,24,25] that BP II (unlike BP I) cannot be supercooled. This indicates that the structures of these two phases are not greatly different and would support the more specific assignment BP II$\leftrightarrow O^2$ and BP I$\leftrightarrow O_c^8$.

V. DISCUSSION

In this paper we have further developed the Landau theory of phase transitions in cholesterics by systematically including the effect of higher harmonics in the structure factor of the free energy. The most important result of this procedure is the appearance of new cubic phases, as summarized in Table IV. Encouragingly, no new structures are introduced by the forth harmonic, strongly indicating that we have succeeded in identifying all cubic phases composed of $m = 2$ harmonics only.

A striking result of our calculations is the extremely small free-energy differences between the various cubic structures. The O_c^8-O^2 (BP I—BP II) boundary, in particular, can shift considerably (see Fig. 4). Thus higher-order terms in the free-energy density,[7] while negligible in other respects, could have a significant effect on the location of the BP I—BP II phase boundary. This could also be the result of small $m \neq 2$ components of the order parameter. Figure 3 should be regarded accordingly.

TABLE IV. Possible cubic structures which are local minima of the Landau free-energy functional as the number of spatial harmonics in the order parameter is increased.

	No. of harmonics		
	One[a]	Two[b]	Three or four[c]
Equilibrium structures	O^5	O^5 O^2, O_a^8	O^5 O^2, O_a^8 O_b^8, O_c^8

[a]Ref. 12.
[b]Refs. 2 and 4.
[c]This paper.

In general, the identification $O^2 \leftrightarrow$ BP II, $O_c^8 \leftrightarrow$ BP I is in accord with the experimental data of Meiboom and Sammon[13] and Stegemeyer and Bergmann[1] on cholesterol derivatives and mixtures. Quantitatively, this is particularly true of the relative intensities and red shift, as shown in Tables II and III. Unfortunately, relative intensity data on other compounds are still lacking. In particular, results on biphenyl mixtures[14,19] are less conclusive than those on the cholestegens (see, e.g, Table III) and may not be consistent with the above assignment.[26] Even with respect to the cholesteryl alkanoates there is not complete agreement. Nicastro and Keyes[18] claim that several of these compounds (valerate, hexanoate, heptanoate, and nonanoate), whose κ values put them in the relatively narrow part of the BP region, do not appear to exhibit a second Bragg back-reflection in the lower section of the BP segment. This could possibly indicate that a O_b^8 structure has been observed. Note that it is in this part of the phase diagram that our calculations (see Table I for $\kappa=0.9$) indicate that $|f_{O^2}-f_{O_b^8}|/f_{O^2}$ is as small as 0.04—0.05. Thus it is here particularly that small energy corrections might result in an O_b^8 phase becoming thermodynamically stable. Further studies would certainly be useful, as these results (for the case of cholesteryl nonanoate) differ sharply from those of Meiboom and Sammon.[13] We also note that the results of Nicastro and Keyes[18] on cholesteryl propionate and butyrate are consistent with O_a^8 as well as O^2 symmetry.

Yet another feature of our theoretical results is their convergence with those of Meiboom *et al.*[10] (see Tables II and III). These two models begin from opposite points of view: The Landau theory is essentially an expansion into the ordered phase from the order-disorder phase boundary. Within a mean-field framework the necessity to take harmonics [and, in principle, terms of higher order than these given in (2)] into consideration arises from the first-order nature of the transition. When the transition is weakly first order (as is the case in cholesterics[20]), then a relatively small number of harmonics suffices to obtain physically realistic results. The disclination theory,[8,10] on the other hand, is basically a zero temperature model in which the order parameter—except in "tubes" located in the immediate vicinity of line disclinations—is constrained to be uniaxial and of constant magnitude. A temperature scale is introduced *ad hoc* by regarding the tubes as being in the disordered phase and using the quadratic term in the Landau expansion to approximate the free-energy density. Outside the tubes the total elastic (Frank) energy is minimized numerically within a unit cell. That results based upon such disparate models are similar, provides, in a sense, external support for the validity of each one. Note further that in the Landau framework the order-parameter field is everywhere analytic as it is simply the Fourier sum of analytic components. We believe this to be the actual physical situation in BP. The nonanalyticity which occurs in disclination models is an unavoidable consequence of using a director representation and is not an intrinsic feature of the problem. It is rather the price that must be paid in order to describe the five-dimensional order parameter by a vectorlike object (the director). Note, for example, that in the director representation one cannot distinguish between negative and positive order parameters; i.e., between those cases in which rodlike molecules favor being oriented in a plane rather than along a unique axis. For example, in the O^5 structure we believe that the molecules are, in the neighborhood of $\langle 111 \rangle$ axes, predominately oriented perpendicular to these directions. This should be an observable effect. In a director model, on the other hand, there is no way to distinguish this type of behavior for that occurring along the O^5 $\langle 100 \rangle$ axes, where the molecules prefer to locally align along these directions. Overall, we believe the Landau approach to be more convenient computationally and to lend itself naturally to a wider range of theoretical results for comparison with experiment.

By restricting our analysis to $m=2$ Fourier components we automatically avoided any consideration of the structure groups T^1 ($P23$), T^3 ($I23$), and T^5 ($I2_13$), which are subgroups of O^2, O^5, and O^8, respectively. In principle one could distinguish between a given group and its respective subgroup by light scattering studies.[4] In practice, however, this is likely to be difficult[4,14] due to the very small Fourier amplitudes expected for $m\neq 2$ components. Thus the structures discussed in this paper are expected to be the experimentally relevant ones. However, we note that contributions from $m\neq 2$ Fourier components and also those from higher-order terms in the Landau free energy can be obtained straightforwardly by utilizing the methods discussed in Sec. II.

Finally, it is clear that amorphous BP III deserves further study and analysis. As noted in the preceding section, Landau theory provides a basis for carrying out such an analysis which would, we believe, complement the study of spatially ordered phases presented here.

ACKNOWLEDGMENTS

We thank M. Kugler, Z. Luz, and D. Mukamel for many useful discussions and comments. We are also grateful to P. P. Crooker, J. W. Doane, P. H. Keyes, M. Marcus, S. Meiboom, and H. Stegemeyer for keeping us informed of their results and for helpful clarifications. This work was supported by a grant from the U.S.-Israel Binational Science Foundation (BSF), Jerusalem, Israel. One of us (R.M.H.) acknowledges support by the Science and Engineering Research Council of the United Kingdom.

APPENDIX A

We here determined the symmetry-allowed values of the phases $\psi_2(hkl)$ for the O^8 space group when $\sigma=h^2+k^2+l^2$ takes the values 2, 4, 6, and 8. We set our coordinate-frame origin on the threefold symmetry axis [111], at its intersection with the twofold symmetry axes [110], [011], and [101]. [This is the point $(\frac{1}{8}\frac{1}{8}\frac{1}{8})$ of the crystallographic unit cell[5] with point symmetry 32.] Then all other phases are related to the set $\psi_2(110)$, $\psi_2(\bar{1}10)$, $\psi_2(200)$, $\psi_2(112)$, $\psi_2(1\bar{1}2)$, $\psi_2(\bar{1}12)$, $\psi_2(\bar{1}\bar{1}2)$, $\psi_2(220)$, and $\psi_2(\bar{2}20)$ by the threefold permutation symmetry. We shall calculate the effect of other symmetry elements of the space group on a component

$$\mu_2(\sigma)e^{i\psi_2(hkl)}[M_2(hkl)]\exp[iq(hx+ky+lz)]\ , \qquad \text{(A1)}$$

of the order parameter as given in (3) and (4). To do this it is necessary to express the $[M_2(hkl)]$ in the coordinate frame of the unit cell. This can be done conveniently using a dyatic notation and writing [we suppress the (hkl) indices]

$$[M_2]_{\alpha\beta}=u_\alpha u_\beta\ , \qquad \text{(A2)}$$

with

$$\hat{u}=(\hat{\xi}+i\hat{\eta})/\sqrt{2}\ . \qquad \text{(A3)}$$

Here $\hat{\xi}$ and $\hat{\eta}$ are real unit vectors, taken such that $\hat{\xi}$, $\hat{\eta}$, and $\hat{\zeta}=(h\hat{x}+k\hat{y}+l\hat{z})/\sigma^{1/2}$ form a local right-handed coordinate system.

Consider first $\psi_2(110)$. The associated local unit vectors are $\hat{\xi}=\hat{z}$, $\hat{\eta}=(\hat{x}-\hat{y})/\sqrt{2}$, and $\hat{\zeta}=(\hat{x}+\hat{y})/\sqrt{2}$. Rotating by π about $[\bar{1}10]$, $x\rightarrow-\hat{y}$, $\hat{y}\rightarrow-\hat{x}$, and $\hat{z}\rightarrow-\hat{z}$. Thus $\hat{\mu}\rightarrow-\hat{\mu}^*$ and $[M_2]\rightarrow[M_2]^*$. The function (A1) with $(hkl)=(110)$ goes to $\mu_2\exp(i\psi_2)[M_2]^*\exp[-iq(x+y)]$ which, by symmetry, must be equal to the complex-conjugate function $\mu_2\exp(-i\psi_2)[M_2]^*\times\exp[-iq(x+y)]$. Thus $\psi_2(110)=0$ or π.

To determine $\psi_2(110)$ we first define the local vectors $\hat{\xi}=-\hat{z}$, $\hat{\eta}=-(\hat{x}+\hat{y})/\sqrt{2}$, and $\hat{\zeta}=(-\hat{x}+\hat{y})/\sqrt{2}$. There is a symmetry element of the space group which consists of a twofold rotation about the axis $[x,\frac{1}{8},-\frac{1}{8}]$, defined with respect to our origin. It takes $\hat{x}\rightarrow\hat{x}$, $\hat{y}\rightarrow-\hat{y}$, and $\hat{z}\rightarrow-\hat{z}$. Also the origin (000) is translated to the point $(0,\frac{1}{4},-\frac{1}{4})$. The function (A1), which initially has the form $\mu_2(\sigma)\exp[i\psi_2(\bar{1}10)][M_2(\bar{1}10)]\exp[iq(-x+y)]$, is transformed to $\mu_2(\sigma)\exp[i\psi_2(\bar{1}10)][M_2(110)]^*\exp[iq(-x-y)-i\pi/2]$. This, by symmetry invariance, must be equal to the function associated with the wave vector $[\bar{1}\bar{1}0]$. It immediately follows that $\psi_2(\bar{1}10)+\pi/2=-\psi_2(110)$ or, $\psi_2(\bar{1}10)=-\pi/2$ when $\psi_2(110)=0$ and $+\pi/2$ when $\psi_2(110)=\pi$.

Turning to $\psi_2(200)$ we define local vectors $\hat{\xi}=\hat{y}$, $\hat{\eta}=z$, and $\zeta=\hat{x}$. Rotating by π about $[\bar{1}10]$, $\hat{x}\rightarrow-\hat{y}$, $\hat{y}\rightarrow-\hat{x}$, and $\hat{z}\rightarrow-\hat{z}$. Then

$$\hat{u}=\hat{y}+i\hat{z}\rightarrow-(\hat{x}+i\hat{z})=\exp(-i\pi/2)(\hat{z}-i\hat{x})$$

and

$$\mu_2\exp[i\psi_2(200)][M_2(200)]\exp(2ix)$$
$$\rightarrow\mu_2\exp[i\psi_2(200)-i\pi][M_2(020)]^*\exp(-2iy)$$
$$=\mu_2\exp[-i\psi(020)][M_2(020)]^*\exp(-2iy)\ .$$

Thus $\psi_2(200)-\pi=-\psi_2(020)=-\psi_2(200)$ and $\psi_2(200)=\pm\pi/2$.

Consider next $\psi_2(112)$. Defining $\hat{\xi}=(-\hat{x}-\hat{y}-\hat{z})/\sqrt{3}$, $\hat{\eta}=(\hat{x}-\hat{y})/\sqrt{2}$, and $\zeta=(\hat{x}+\hat{y}+2\hat{z})/\sqrt{6}$ and rotating by π about $[\bar{1}10]$, it is straightforward to show that $\psi_2(112)=0$ or π. The phase $\psi_2(\bar{1}\bar{1}2)$ [with $\hat{\xi}=(\hat{x}+\hat{y}+\hat{z})/\sqrt{3}$, $\hat{\eta}=(-\hat{x}+\hat{y})/\sqrt{2}$, $\hat{\zeta}=(-\hat{x}-\hat{y}-2\hat{z})/\sqrt{6}$] is, by a twofold rotation about $[\frac{1}{8},-\frac{1}{8},z]$, found to be equal to $\psi_2(112)$. Similarly, the phases $\psi_2(1\bar{1}2)$ about $\psi_2(\bar{1}12)$ [with $\hat{\xi}=(-\hat{x}+\hat{y}+\hat{z})/\sqrt{3}$, $\hat{\eta}=(-\hat{x}-\hat{y})/\sqrt{2}$, $\hat{\zeta}=(\hat{x}-\hat{\eta}+2\hat{z})/\sqrt{6}$ and $\hat{\xi}=(\hat{x}-\hat{y}+\hat{z})/\sqrt{3}$, $\hat{\eta}=(\hat{x}+\hat{y})/\sqrt{2}$, $\hat{\zeta}=(-\hat{x}+\hat{y}+2\hat{z})/\sqrt{6}$, respectively] are found by a π rotation about [110] to satisfy $\psi_2(1\bar{1}2)=-\psi_2(\bar{1}12)$. Further, the former, by a π rotation about $[x,\frac{1}{8},-\frac{1}{8}]$, must be equal to $-\pi/2$ if $\psi_2(\bar{1}\bar{1}2)=0$ and $+\pi/2$ if $\psi_2(\bar{1}\bar{1}2)=\pi$. We thus have the two possible sets of values:

$$\psi_2(112)=\psi_2(\bar{1}\bar{1}2)=0;\quad \psi_2(1\bar{1}2)=-\psi_2(\bar{1}12)=-\pi/2\ ,$$

or

TABLE V. Symmetry-allowed phase angles for the low-lying $m=2$ Fourier components of the O^2, O^5, and O^8 structure factors. All others may be obtained by cyclic permutation. The first of the two given values is that corresponding to the local minimum of the Landau free energy except as noted below.

Structure	Phases $\psi_m(hkl)$	Symmetry-allowed values
O^2	$\psi_2(100)$	$0;\pi$[a]
	$\psi_2(100)=\psi_2(\bar{1}10)$	$\pi;0$
O^5	$\psi_2(110)=\psi_2(\bar{1}10)$	$0;\pi$
	$\psi_2(112)=\psi_2(1\bar{1}2)=\psi_2(\bar{1}12)=\psi_2(\bar{1}\bar{1}2)$	$0;\pi$
	$\psi_2(220)=\psi_2(\bar{2}20)$	$0;\pi$[b]
O^8	$\psi_2(110)=-\psi_2(\bar{1}10)-\frac{1}{2}\pi$	0[c]$;\pi$[d]
	$\psi_2(200)$	$-\frac{1}{2}\pi;\frac{1}{2}\pi$
	$\psi_2(112)=\psi_2(\bar{1}\bar{1}2)=-\psi_2(1\bar{1}2)-\frac{1}{2}\pi=\psi_2(\bar{1}12)-\frac{1}{2}\pi$	$0;\pi$
	$\psi_2(220)=\psi_2(\bar{2}20)+\pi$	$0;\pi$[e]

[a]Both angles give equal free energies. See Ref. 6.
[b]In some cases this angle should be used (see Table I).
[c]This choice corresponds to the O_a^8 and O_b^8 structures.
[d]This choice corresponds to the O_c^8 structure.
[e]In some cases this angle should be used for O_c^8 (see Table I).

$$\psi_2(112)=\psi_2(\bar{1}\bar{1}2)=\pi;\quad \psi_2(1\bar{1}2)=-\psi_2(\bar{1}12)=+\pi/2\ .$$

Finally, we turn to the phases $\psi_2(220)$ and $\psi_2(\bar{2}20)$. Using the same basis vectors and symmetry operations employed for $\psi_2(110)$ and $\psi_2(\bar{1}10)$, respectively, we find that $\psi_2(220)=0$ or π and that $\psi_2(\bar{2}20)=\psi_2(220)+\pi$. This completes our determination of the symmetry-allowed phases for the four lowest-lying wave vectors of O^8. The symmetry-allowed relevant phases for O^2, O^5, and O^8 structures are summarized in Table V.

APPENDIX B

In the theoretical analysis carried out in Sec. II, a scaled and dimensionless form of the Landau free-energy functional was used. This was particularly convenient since the term in (2) proportional to c_2 did not contribute for the structures studied. For experimental purposes, however, a formulation in terms of directly measurable quantities may be more useful. This is given here.

Three of the scaled quantities introduced in (7) satisfy this requirement. The first, q_C, is the usual cholesteric wave vector and is related to the Bragg back-reflection wavelength in air by $\lambda_C^{\rm AIR}=4\pi n/q_C$, where n is the index of refraction. The other two, ξ_R and t, are the correlation length for a racemic ($q_C=0$) mixture on the isotropic-racemic phase boundary T_R and the difference in temperature between this boundary and T_R^*, which is obtained by extrapolating the disordered-phase correlation-length divergence to infinity. That is,

$$t=(T-T_R^*)/(T_R-T_R^*)\equiv(T-T_R^*)/\Delta T_R\ . \tag{B1}$$

Defining $\epsilon_{||},\epsilon_\perp$ as the experimentally accessible dielectric constants parallel and perpendicular to the nematic axis for the racemic mixture, it is straightforward to show that

$$\beta/\gamma=4(\epsilon_{||}-\epsilon_\perp)\,|_{T=T_R}\equiv 4(\Delta\epsilon)\ . \tag{B2}$$

We therefore choose as our normalized order parameter

$$\tilde{\epsilon}_{ij}\equiv\epsilon_{ij}/\Delta\epsilon\ , \tag{B3}$$

noting that $\mu_{ij}=\sqrt{6}\tilde{\epsilon}_{ij}/4$. Finally, a measurable unit of energy or energy density is needed. Two possible choices are the racemic Frank elastic energy coefficient and the latent heat associated with the isotropic-racemic phase transition. For the former, we note that for the case of a locally uniaxial system the elastic energy density term in (2) becomes

$$\tfrac{1}{2}c_1\epsilon_{ij,l}^2=\tfrac{3}{4}(\beta^4/36\gamma^3)\xi_R^2\mu^2(n_{i,l})^2\ , \tag{B4}$$

where $\hat{n}$ is the director. Using $\mu(T=T_R)=\frac{1}{2}$, we have for the corresponding Frank constant

$$K=(\beta^4/96\gamma^3)\xi_R^2\ . \tag{B5}$$

Since the three Frank constants are not equal, the appropriate one to use in (B5) is that for twist, as this is the dominant contribution to the elastic energy in cholesteric systems.

The alternate choice, latent heat, is given by

$$\begin{aligned}L&=T_R(\partial F/\partial T)_{T=T_R}\\&=T_R(\beta^4/36\gamma^3)[\partial(\tfrac{1}{4}t\mu^2)/\partial T]_{T=T_R}\\&=(\beta^4/576\gamma^3)(T_R/\Delta T_R)\ .\end{aligned} \tag{B6}$$

Defining a normalized length $\rho=r/\xi_R$ and volume $v=V/\xi_R$ and using (2), (B1)–(B3), and either (B5) or (B6), the following expression for the average Landau free-energy density is obtained:

$$\begin{aligned}F=(A/v)\int d\vec{\rho}[\,&\tfrac{1}{2}(\tilde{\epsilon}_{ij}^2-2\kappa e_{ijl}\tilde{\epsilon}_{in}\tilde{\epsilon}_{jn,l}+\tilde{\epsilon}_{ij,l}^2)\\&-3\tilde{\epsilon}_{ij}\tilde{\epsilon}_{jl}\tilde{\epsilon}_{li}+\tfrac{3}{4}(\tilde{\epsilon}_{ij}^2)^2]\ ,\end{aligned} \tag{B7}$$

with all derivatives now with respect to normalized coordinates and

$$\begin{aligned}&A=K/2\xi_R^2\\ \text{or}\quad&\\&A=3L\Delta T_R/T_R\ .\end{aligned} \tag{B8}$$

The quantities q_C, ξ_R, T_R, T_R^*, K, and L are all experimentally accessible and both expressions in (B8) yield approximately equal values for A.[20] Note particularly that the normalized free energy $F/(A/v)$ is a *universal function* of κ and t.

APPENDIX C

A nonpolarized incident beam may be regarded as composed of right- and left-hand circularly polarized components of equal magnitude. As essentially only one of those is Bragg scattered in cubic cholesteric BP, let us consider a beam i with 100% relevant polarization. Assuming that multiple scattering is negligible, the relative intensity of the polarized transmitted beam at a Bragg backscattering wavelength λ_σ for a sample of thickness D will be

$$i(\sigma;D)/i(\sigma;0)=e^{-\alpha D}\ , \tag{C1}$$

where, from (17) and (18), $\alpha(\sigma)$ is proportional to $\sigma^{1/2}\epsilon_2^2(\sigma)$. Thus the relative step in the polarized beam intensity is

$$\frac{i(\sigma;0)-(\sigma;D)}{i(\sigma;D)}=1-e^{-\alpha D}\ , \tag{C2}$$

and is simply proportional to $\alpha(\sigma)$ as $D\to 0$. In general,

$$\frac{\alpha(\sigma_2)}{\alpha(\sigma_1)}=\frac{\sigma_2^{1/2}\epsilon_2^2(\sigma_2)}{\sigma_1^{1/2}\epsilon_2^2(\sigma_1)}=\frac{\ln[i(\sigma_2;D)/i(\sigma_2;0)]}{\ln[i(\sigma_1;D)/i(\sigma_1;0)]}\ . \tag{C3}$$

Relative to the total *unpolarized* intensity I_0 transmitted in the disordered phase, we have

$$i(\sigma;l)=I(\sigma;l)/I_0-0.5;\quad l=0,D\ . \tag{C4}$$

Here, $I(\sigma;0)$ and $I(\sigma;D)$ are the (in general, partially circularly polarized) transmitted intensities measured at wavelengths slightly greater and less than λ_σ, respectively. Using (C3) and (C4) the observed intensity ratios can be compared with the calculated $\epsilon_2^2(\sigma_2)/\epsilon_2^2(\sigma_1)$ ratios. In general, however, the measured intensities would have to be corrected for multiple scattering and wavelength-dependent anomalous scattering and depolarization before a quantitative comparison could be made.[4(c)]

*Permanent address: Department of Electronics, Weizmann Institute of Science, Rehovot 76100, Israel.

†Permanent address: Department of Electronics, Weizmann Institute of Science, Rehovot, Israel.

[1]For an experimental review and references to earlier work, see H. Stegemeyer and K. Bergmann, in *Liquid Crystals of One and Two Dimensional Order,* edited by W. Helfrich and G. Heppke (Springer, Berlin, 1980), p. 161. A more recent review is P. P. Crooker, Mol. Cryst. Liq. Cryst. **98**, 31 (1983).

[2]H. Grebel, R. M. Hornreich, and S. Shtrikman, Phys. Rev. A **28**, 1114 (1983); **28**, 3669(E) (1983). Their paper contains a comprehensive list of references to the extensive experimental and theoretical work on cholesteric blue phases published from 1980 to 1983.

[3]P. G. de Gennes, Mol. Cryst. Liq. Cryst. **12**, 193 (1971).

[4]R. M. Hornreich and S. Shtrikman, (a) Phys. Lett. **82A**, 345 (1981); (b) Phys. Rev. A **28**, 1791 (1983); **28**, 3669(E) (1983). See also (c) V. M. Belyakov, V. E. Dmitrienko, and S.M. Osadchii, Zh. Eksp. Teor. Fiz. **83**, 585 (1982); **84**, 1920(E) (1982) [Sov. Phys.—JETP **56**, 322 (1982); **57**, 1117(E) (1982)].

[5]*International Tables for X-Ray Crystallography* (Kynoch, Birmingham, 1965), Vol. I.

[6]This degeneracy in the $\mu_2(1)$ phase angle is removed when couplings to higher-order allowed harmonics are taken into account.

[7]R. M. Hornreich and S. Shtrikman, Phys. Lett. **84A**, 20 (1981). [In Eq. (6) replace $1+\alpha$ by α and multiply the final term by $2k_0$. In Eq. (7) replace $1+\alpha$ by 2α and $1-\alpha$ by $(1-\alpha)/2$. The initial slope is $\omega_p=1.57/3.37$. All conclusions are unaffected.]

[8]S. Meiboom, J. P. Sethna, P. W. Anderson, and W. F. Brinkman, Phys. Rev. Lett. 46, 1216 (1981); S. Meiboom, M. Sammon, and W. F. Brinkman, Phys. Rev. A **27**, 438 (1983).

[9]R. M. Hornreich, M. Kugler, and S. Shtrikman, Phys. Rev. Lett. **48**, 1404 (1982).

[10]S. Meiboom, M. Sammon, and D. W. Berreman, Phys. Rev. A **28**, 3553 (1983). In their paper, the notation $O^{8(+)}$ and $O^{8(-)}$ is used for our O_b^8 and O_c^8, respectively. See also D. W. Berreman, in *Liquid Crystals and Ordered Fluids,* edited by R. C. Griffin and J. F. Johnson (Plenum, New York, 1982), Vol. 4.

[11]A. Saupe, Mol. Cryst. Liq. Cryst. **7**, 59 (1969).

[12]R. M. Hornreich and S. Shtrikman, (a) Bull. Israel Phys. Soc. **25**, 46 (1979); (b) J. Phys. (Paris) **41**, 335 (1980); **42**, 367(E) (1981); (c) in *Liquid Crystals of One and Two-Dimensional Order,* edited by W. Helfrich and G. Heppke (Springer, Berlin, 1980), p. 185.

[13]S. Meiboom and M. Sammon, Phys. Rev. Lett. **44**, 882 (1980); Phys. Rev. A **42**, 468 (1981).

[14]D. L. Johnson, J. H. Flack, and P. P. Crooker, Phys. Rev. Lett. **45**, 641 (1980); J. H. Flack and P. P. Crooker, Phys. Lett. **82A**, 247 (1981); J. H. Flack, P. P. Crooker, and R. V. Svoboda, Phys. Rev. A **26**, 723 (1982).

[15]M. Marcus, J. Phys. (Paris) **42**, 61 (1981); M. Marcus and J. W. Goodby, Mol. Cryst. Liq. Cryst. Lett. **72**, 297 (1982).

[16]C. C. Yang, Phys. Rev. Lett. **28**, 955 (1972).

[17]Y. Poggi, P. Atten, and J. C. Pilippini, Mol. Cryst. Liq. Cryst. **37**, 1 (1976).

[18]P. H. Keyes, A. J. Nicastro, and E. M. McKinnon, Mol. Cryst. Liq. Cryst. **67**, 59 (1981); A. J. Nicastro and P. H. Keyes, Phys. Rev. A **27**, 431 (1983).

[19]J. Her, B. B. Rao, and J. T. Ho, Phys. Rev. A **24**, 3272 (1981); J. Her and J. T. Ho, in *Liquid Crystals and Ordered Fluids,* edited by A. C. Griffin and J. F. Johnson (Plenum, New York, 1982), Vol. 4.

[20]See, e.g., M. J. Stephen and J. P. Straley, Rev. Mod. Phys. **46**, 617 (1974).

[21]H. Grebel, R. M. Hornreich, and S. Shtrikman, Phys. Rev. A **28**, 2544 (1983).

[22]E. T. Samulskii and Z. Luz, J. Chem. Phys. **73**, 142 (1980).

[23]Z. Yaniv, G. Childichimo, and J. W. Doane, Phys. Rev. A **28**, 3012 (1983).

[24]H. Onusseit and H. Stegemeyer, Z. Naturforsch. Teil A **36**, 1083 (1981).

[25]M. Marcus, Phys. Rev. A **25**, 2272 (1982).

[26]Recent results [K. Tanimoto and P. P. Crooker, Phys. Rev. A **29**, 1566 (1984)] indicate that BP II in biphenyl mixtures is bcc.

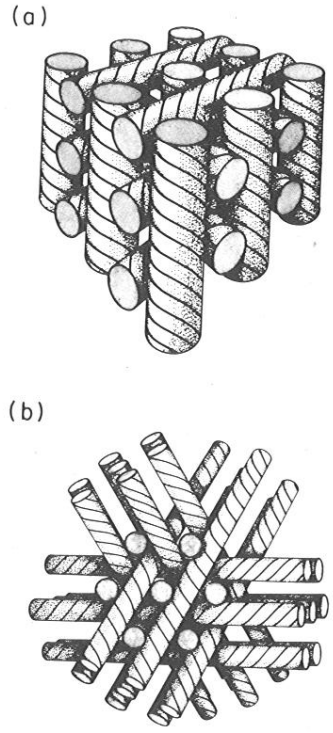

FIG. 6. The (a) O^2 and (b) O_a^8, O_b^8 cubic structures, showing how they can be visualized as appropriate interlaced assemblies of the curling-mode configuration cylinders of Fig. 5.